

$K^{*0}(892)$ and $\phi(1020)$ resonance production at RHIC

Lokesh Kumar^{1,a} (for STAR Collaboration)

¹Department of Physics, Panjab University, Chandigarh, INDIA-160014

Abstract. The measurement of resonance production in ultrarelativistic heavy-ion collisions provides a glimpse of the hadronic medium properties and its evolution at different stages. Resonances decaying into hadrons are used to estimate the time span and hadronic interaction cross section in the hadronic phase between chemical and kinetic freeze-out. Specifically, the comparison of $K^{*0}(892)$ and $\phi(1020)$ resonances is interesting as the lifetimes of these particles differ by about a factor of 10. Moreover, the nuclear modification factor and azimuthal anisotropy measurements of mesonic resonances, which measure parton energy loss in medium and reflect partonic collectivity, can also probe particle-species and mass ordering.

The $K^{*0}(892)$ and $\phi(1020)$ resonance production at mid-rapidity ($|y| < 0.5$), measured in high energy (Au+Au, Cu+Cu, d+Au and $p + p$) collisions at RHIC with the STAR experiment, reconstructed by their hadronic decay in $K\pi$ and KK , respectively, are discussed. Mesons' spectra, yields, mean transverse momentum $\langle p_T \rangle$, nuclear modification factor, and azimuthal anisotropy are discussed as a function of centrality and collision energy.

1 Introduction

Quantum Chromodynamics (QCD) predicts a phase transition from nuclear matter to a state of deconfined matter, called the quark gluon plasma (QGP), at high temperature and energy density [1]. High energy heavy-ion collisions provide ideal scenario for the formation of the QGP [2]. The study of resonance production can be a useful tool in understanding the properties of the system formed in heavy-ion collisions. Since their lifetimes are comparable to that of fireball, resonance particles are expected to decay, rescatter, and regenerate to the kinetic freeze-out state (vanishing elastic collisions). As a result, their characteristic properties may be modified due to in-medium effects [3]. The study of resonance particles can provide the time span and hadronic interaction cross-section of the hadronic phase between chemical (vanishing inelastic collisions) and kinetic freeze-out [4].

Comparisons of K^{*0} and ϕ mesons are interesting since their lifetimes differ by a factor of 10 [5]. K^{*0} has a lifetime ~ 4 fm/c [6], comparable with that of the fireball, so it is expected to suffer changes from the in-medium effects. There are two competing processes affecting K^{*0} yield, rescattering that reduces the K^{*0} yield and regeneration that may lead to increase in K^{*0} yield [7]. As a result, it is expected that K^{*0}/K should change as a function of centrality, i.e., increase due to regeneration or decrease due to rescattering. On the other hand, ϕ mesons are expected to freeze-out early [2] and have a comparatively larger lifetime (~ 45 fm/c) than K^{*0} , so they may not undergo rescattering and regeneration effects. As a result, the ϕ/K ratio should remain constant as a function of centrality.

^ae-mail: lokesh@rf.rhic.bnl.gov

Another interesting property of the ϕ meson is that being a meson, it has a mass comparable to that of protons and Λ , which are baryons. Studying the ϕ meson (e.g., elliptic flow) along with these baryons and other mesons may give information on quark coalescence or the partonic phase at the top RHIC energy [8]. Once the partonic phase is established at higher energies, one would expect the turn-off of partonic phase or decrease of dominance of the partonic interactions when the energy is decreased. This is one of the goals of the RHIC Beam Energy Scan (BES) program [9].

2 Experimental Detail

The results presented here are mainly from the Solenoidal Tracker At RHIC (STAR) experiment. The STAR detector has a coverage of 2π in azimuth and pseudorapidity $|\eta| < 1$. The data sets include Au+Au, Cu+Cu, d+Au, and $p + p$ collisions for energies $\sqrt{s_{NN}} = 62.4$ and 200 GeV. Results from the Beam Energy Scan phase-I, that include data from Au+Au collisions at $\sqrt{s_{NN}} = 7.7, 11.5, 19.6, 27,$ and 39 GeV, are also presented. The STAR Time Projection Chamber (TPC) is the main detector used for particle identification by measuring the particle energy loss [10].

The centrality selection is done using the uncorrected charged track multiplicity measured in the TPC within $|\eta| < 0.5$ and comparing with Monte-Carlo Glauber simulations [11]. Both K^{*0} and ϕ resonances are reconstructed via their hadronic decay channels: $K^{*0} \rightarrow K\pi$ and $\phi \rightarrow KK$. These daughter particles are identified using the TPC as mentioned above. K^{*0} and ϕ mesons are reconstructed by calculating invariant mass for each unlike-sign $K\pi$ and KK , respectively, in an event. The resultant distribution consists of the true signal (K^{*0} or ϕ) and contributions arising from the random combination of unlike sign $K\pi$ and KK pairs. To extract the K^{*0} or ϕ yield, the large random combinatorial background must be subtracted from the unlike sign $K\pi$ or KK pairs. The random combinatorial background distribution is obtained using the mixed-event technique [12]. In the mixed event technique, the background distribution is built with uncorrelated unlike-sign $K\pi$ or KK pairs from different events. The generated mixed events distribution is then properly normalized to subtract the background from the same event unlike-sign invariant mass spectrum.

3 Results and Discussions

Figure 1 shows the invariant yields versus transverse momentum p_T of K^{*0} (left plot) and ϕ (right plot) in Au+Au collisions at 62.4 and 200 GeV, respectively for different collision centralities [13, 14]. From these distributions, dN/dy and average transverse momentum $\langle p_T \rangle$ can be obtained. These quantities provide important information about the system formed in high energy collisions. It is observed that dN/dy per participating nucleon pair for K^{*0} increases with increasing energy. ϕ meson yields per participating nucleon increases with increasing energy and centrality [13, 15]. dN/dy per participating nucleon pair increases from $pp, d+Au$ to Au+Au collisions at 200 GeV for both K^{*0} and ϕ mesons. Comparing $\langle p_T \rangle$ of K^{*0} with pions, kaons, and protons in Au+Au collisions at 200 GeV, suggests that it is greater than that of pions and kaons but similar to that of protons, reflecting mass dependence or collectivity [16]. When K^{*0} $\langle p_T \rangle$ is compared between pp and Au+Au collisions at 200 GeV, it is found to be larger in Au+Au collisions, suggesting larger radial flow. In general, $\langle p_T \rangle$ increases with particle mass, showing a collective behavior [15].

3.1 Rescattering effect

Figure 2 (left plot) shows ratio of K^{*0}/K^- as a function of $dN_{ch}/d\eta$, which reflects the centrality [17]. The right plot shows the double ratio i.e. ratio of K^{*0}/K^- in heavy-ion collisions over that in pp

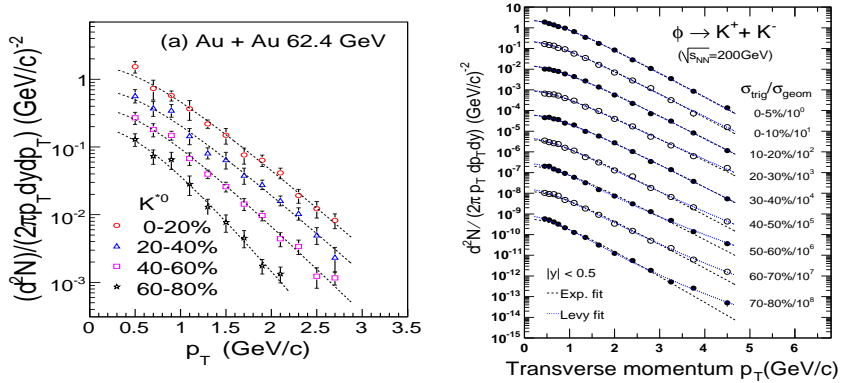


Figure 1. Left: Invariant yields versus p_T for K^{*0} in Au+Au collisions at 62.4 GeV for different centralities [13]. Right: Invariant yields versus p_T for ϕ mesons in Au+Au collisions at 200 GeV for different centralities [14].

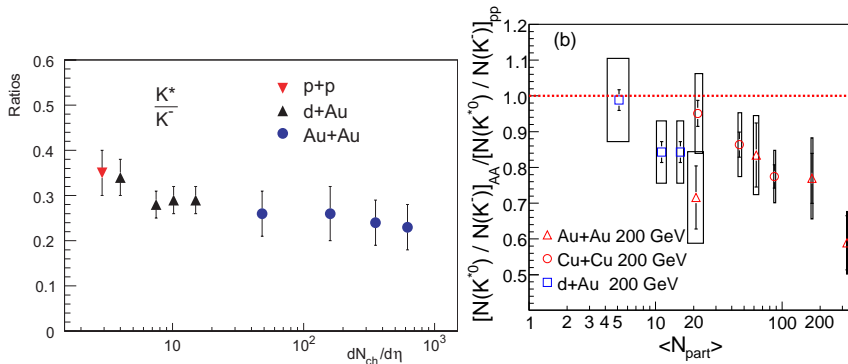


Figure 2. Left: K^{*0}/K^- ratio in $p + p$ and various centralities in $d+Au$ and $Au+Au$ collisions as a function of $dN_{ch}/d\eta$ [17]. Right: K^{*0}/K^- ratio in $Au+Au$, $Cu+Cu$, and $d+Au$ collisions divided by that in $p + p$ collisions at $\sqrt{s_{NN}} = 200$ GeV as a function of $\langle N_{part} \rangle$ [13].

collisions [13]. One can see that the ratio K^{*0}/K^- decreases as a function of increasing number of participating nucleons as well as decreases from pp , $d+Au$, to central $Au+Au$ collisions. This decrease in the K^{*0}/K^- ratio may be attributed to the rescattering of daughter particles of K^{*0} .

Figure 3 (left plot) shows ratio of ϕ/K^- as a function of number of participating nucleons [15]. The ratio remains flat as a function of collision centrality, suggesting that there is a negligible rescattering effect for ϕ . The results are also compared with UrQMD model which assumes kaon coalescence as the dominant mechanism for ϕ production. As seen, the data rules out the kaon coalescence as dominant mechanism for the ϕ -meson production. The right plot shows the double ratio i.e. ratio of ϕ/K^{*0} in heavy-ion collisions over that in pp collisions. It shows that the ratio increases with increasing N_{part} [17]. This increase might be either due to rescattering of daughter of K^{*0} or strangeness enhancement for ϕ . Since, we already see that K^{*0} shows rescattering effect, this increase is most likely due to the rescattering effect for K^{*0} .

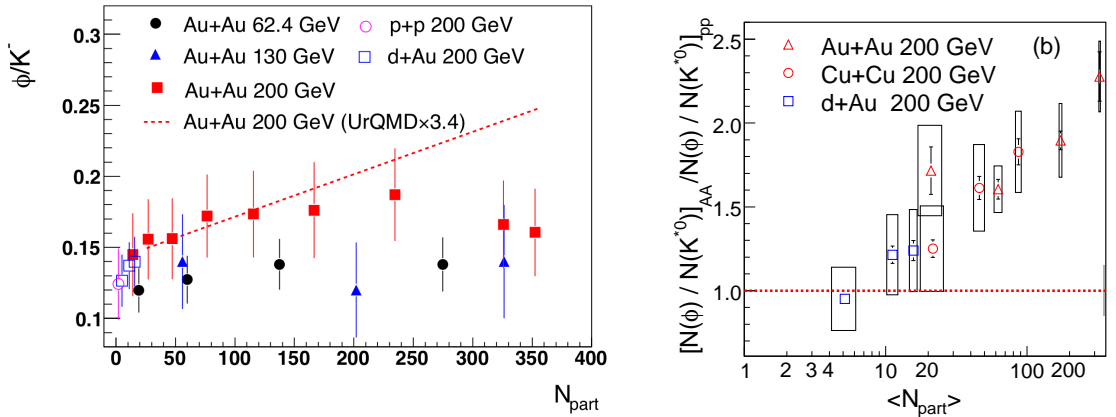


Figure 3. Left: ϕ/K^- ratio in $p + p$ and various centralities in $d+Au$ and $Au+Au$ collisions as a function of $\langle N_{\text{part}} \rangle$ [15]. The dashed line shows results from UrQMD model calculations. Right: ϕ/K^{*0} ratio in $Au+Au$, $Cu+Cu$, and $d+Au$ collisions divided by that in $p + p$ collisions at $\sqrt{s_{NN}} = 200$ GeV as a function of $\langle N_{\text{part}} \rangle$ [17].

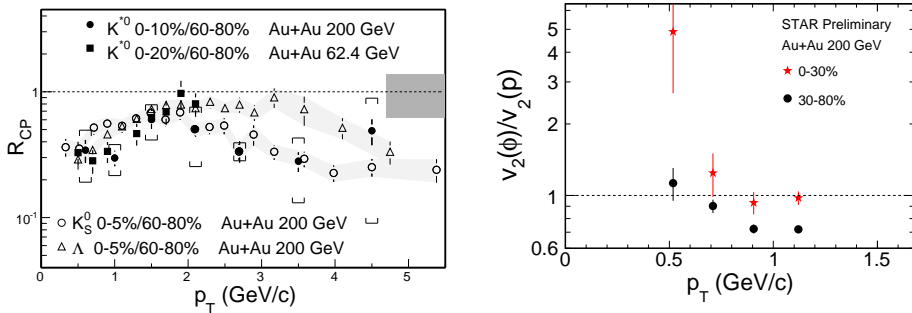


Figure 4. Left: R_{CP} of K^{*0} as a function of p_T in $Au+Au$ collisions at 200 GeV and 62.4 GeV compared with that of K_S^0 and Λ at 200 GeV [13]. Right: $v_2(\phi)/v_2(p)$ ratio as a function of p_T in $Au+Au$ collisions at two different centralities [19].

Figure 4 (left plot) shows the nuclear modification factor (R_{CP}), defined as yields in central collisions to that in peripheral collisions scaled by the number of binary collisions [13, 18]. At low p_T ($p_T < 1.8$ GeV/c), we observe that R_{CP} of K^{*0} is less than that of K_S^0 (also a meson) and Λ (having almost similar mass). The lower value of R_{CP} of K^{*0} might be due to the rescattering of daughter particles of K^{*0} at low p_T in the medium. The right plot shows the elliptic flow parameter v_2 of ϕ divided by v_2 of proton as a function of p_T for high statistics $Au+Au$ data at 200 GeV for two different centralities [19]. At low p_T , we observe that this ratio is not unity. Since the ϕ mass is similar to the proton mass, we expect a similar v_2 for ϕ and proton at low p_T due to mass-ordering. However, data show that the mass ordering is broken at low p_T , which might be due to rescattering of protons at low p_T as suggested in Ref. [20].

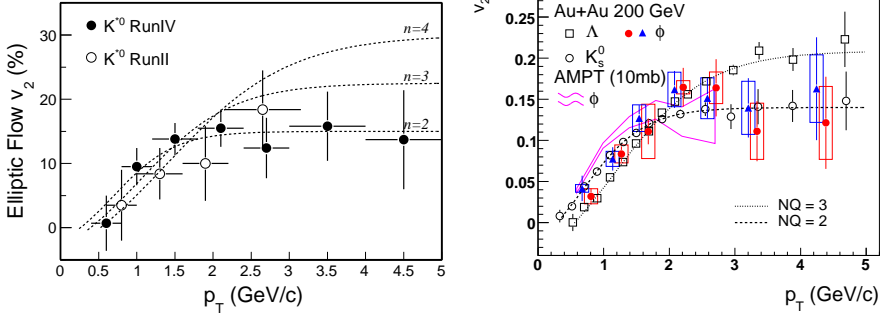


Figure 5. Left: K^{*0} v_2 as a function of p_T in minimum bias Au+Au collisions at 200 GeV [13]. The dashed lines represent the v_2 of hadrons with different numbers of constituent quarks. Right: p_T dependence of v_2 of ϕ , Λ , and K_S^0 in Au+Au collisions (0-80%) at 200 GeV [14]. The magenta curved band represents the v_2 of the ϕ meson from the AMPT model with a string melting mechanism. The dash and dot curves represent parametrizations for number of constituent quarks, $NQ = 2$ and $NQ=3$, respectively.

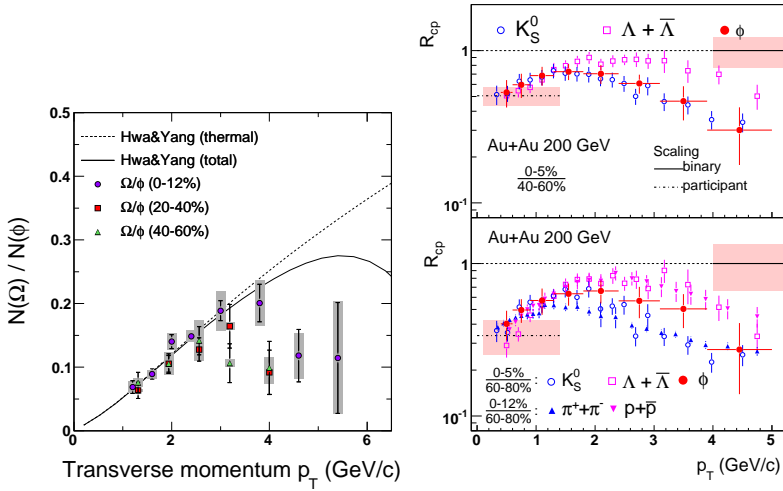


Figure 6. Left: Ω/ϕ ratio versus p_T for three centralities in $\sqrt{s_{NN}} = 200$ GeV Au+Au collisions [14]. The solid and dashed lines represent recombination model predictions for central collisions for total and thermal contributions, respectively. Right: p_T dependence of the nuclear modification factor R_{CP} ϕ meson compared with K_S^0 and Λ in Au+Au 200 GeV collisions [15]. The top and bottom panels present R_{CP} from midperipheral and most-peripheral collisions, respectively.

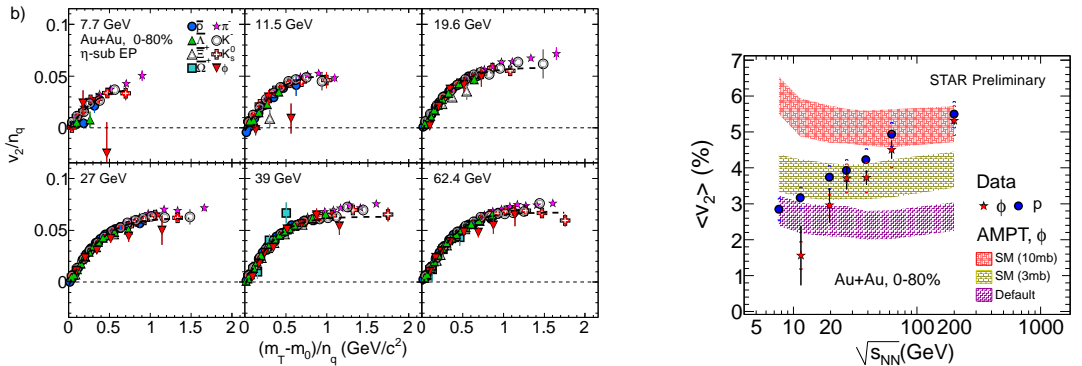


Figure 7. Left: v_2/n_q as a function of $(m_T - m_0)/n_q$ for different particles in Au+Au collisions at $\sqrt{s_{NN}} = 7.7, 11.5, 19.6, 27, 39$ and 62.4 GeV [21]. Right: The p_T integrated ϕ meson and proton v_2 for Au+Au minimum bias (0–80%) collisions at mid-rapidity $|y| < 1.0$ at RHIC as a function of $\sqrt{s_{NN}}$ [22]. The ϕ meson v_2 values are compared with corresponding AMPT model calculations at various beam energies.

3.2 Quark coalescence and partonic effects

Figure 5 (left plot) shows the v_2 versus p_T for K^{*0} in Au+Au collisions at 200 GeV [13]. The various curves show the number of constituent quarks ($n=2$ for mesons and 3 for baryons). We observe that the K^{*0} v_2 follows the $n=2$ parametrization suggesting quark coalescence for their production [8]. The right plot shows the v_2 versus p_T for the ϕ meson compared with K_S^0 and Λ along with number-of-constituent-quark parameterizations [14]. We see that the ϕ meson follows the K_S^0 behavior and the $n=2$ curve. Since ϕ meson is not formed via kaon coalescence and undergoes less hadronic interaction (as discussed before), the observed v_2 of ϕ is due to the partonic phase. These results also suggest that heavier quarks flow as strongly as lighter quarks.

Figure 6 (left plot) shows the Ω/ϕ ratio as a function of transverse momentum p_T for three different centralities in Au+Au collisions at 200 GeV [14]. Data are compared with the model calculations which assume that Ω and ϕ are produced from thermal s quarks coalescence in the medium. The results show that the coalescence model reproduces the data at low p_T . The right plot shows the nuclear modification factor R_{CP} of ϕ for 0–5%/40–60% (top panel) and 0–5%/60–80% (bottom panel), compared with R_{CP} of different particles [15]. A suppression of R_{CP} at high p_T has been suggested to be the signature of dense medium or quark gluon plasma formation in heavy-ion collisions. Together with Fig. 4 (left plot), above results suggest that both K^{*0} and ϕ R_{CP} show suppression at high p_T , suggesting dense medium formation at the top RHIC energy.

3.3 Energy dependence of partonic interactions

In the previous subsection, we have established the partonic nature of the system formed at the top RHIC energy. It is interesting to see what happens to this partonic nature when the collision energy is decreased. RHIC Beam Energy Scan (BES) allows to check this energy dependence.

Figure 7 (left plot) shows the v_2 scaled by the number of constituent quarks (ncq) plotted versus $m_T - m$ divided by number of constituent quarks. Results are shown for 7.7, 11.5, 19.6, 27, 39, and 62.4 GeV, and for various particles that include mesons and baryons [21]. We observe that all particles

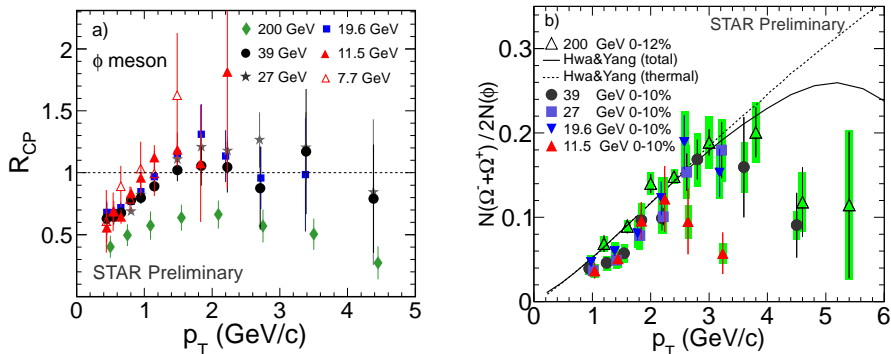


Figure 8. Left: R_{CP} of ϕ as a function of p_T in Au+Au collisions at various beam energies [19]. Right: Ratio $N(\Omega^- + \Omega^+) / (2N(\phi))$ as a function of p_T in central Au+Au collisions at $\sqrt{s_{NN}} = 11.5$ –200 GeV [22–24]. The curves represent model calculations by Hwa and Yang for $\sqrt{s_{NN}} = 200$ GeV.

follow nq scaling down to 19.6 GeV. However, at 11.5 GeV and below ϕ mesons deviate from this scaling. Since ϕ meson has a small hadronic interaction cross-section [2], this small ϕv_2 may suggest less partonic contributions at lower energies. However, as can be seen, higher statistics are needed at lower energies to make definite conclusions. The right plot shows the the v_2 of ϕ mesons compared to corresponding AMPT model calculations [22]. The $\langle v_2 \rangle$ values from the model is constant for all the energies at a given parton-parton interaction cross-section. This is expected because it is the interactions between minijet partons in the AMPT models that generate v_2 . The v_2 of ϕ mesons for $\sqrt{s_{NN}} > 19.6$ GeV can be explained by the AMPT model with string melting enabled (AMPT-SM). The AMPT-SM model with 10 mb parton-parton cross-section fits the data at $\sqrt{s_{NN}} = 62.4$ and 200 GeV, whereas a reduced value of parton-parton cross-section of 3 mb is needed to describe the data at $\sqrt{s_{NN}} = 27$ and 39 GeV. On the other hand, the data at $\sqrt{s_{NN}} = 11.5$ GeV are explained within the default version of the AMPT model without the partonic interactions. These model results along with data indicate that for $\sqrt{s_{NN}} < 11.5$ GeV, the hadronic interaction plays a dominant role, whereas above 19.6 GeV contribution from partonic interactions increases.

Figure 8 (left plot) Nuclear modification factor R_{CP} (0–10%/40–60%) of ϕ meson at different BES energies along with 200 GeV ((0–5%/40–60%)) [19]. We observe that $R_{CP} \geq 1$ for beam energies $\sqrt{s_{NN}} \leq 19.6$ GeV. The right plot shows the Ω/ϕ ratio versus p_T for different energies from $\sqrt{s_{NN}} = 11.5, 19.6$ GeV, up to 200 GeV [22–24]. We observe that 19.6, 27 and 39 GeV follow the same behavior as 200 GeV, however, the ratio at 11.5 GeV show different trend i.e. the ratio turns down at lower p_T when compared to higher energies. This may suggest different particle production phenomenon at 11.5 GeV compared to higher energies.

4 Summary

In summary, $K^{*0}(892)$ and $\phi(1020)$ resonance production at RHIC is discussed. The K^{*0}/K^- ratio decreases as a function of N_{part} , R_{CP} of K^{*0} is less than that of K_S^0 and Λ at low p_T , and the ϕ/K ratio remains constant as a function of centrality. These results suggest rescattering effect for K^{*0} and may be negligible rescattering effect for ϕ mesons. The number-of-constituent-quark scaling is observed

for both K^{*0} and ϕ , possibly indicating partonic nature of system formed at the top RHIC energy. Similarly, the quark coalescence model explains the Ω/ϕ ratio at low p_T . The energy dependence of various observables suggest that the system formed at lower energies may be hadron dominant. As an example, ϕ meson v_2 does not follow ncq-scaling for $\sqrt{s_{NN}} \leq 11.5$ GeV. v_2 of ϕ mesons compared with model results indicate that for $\sqrt{s_{NN}} < 11.5$ GeV the hadronic interaction plays a dominant role. Energy dependence of Ω/ϕ ratio versus p_T suggests a change of particle production at $\sqrt{s_{NN}} = 11.5$ GeV and the ϕ meson $R_{CP} \geq 1$ for beam energies $\sqrt{s_{NN}} \leq 19.6$ GeV.

References

- [1] F. Karsch, Nucl. Phys. A **698**, 199 (2002).
- [2] J. Adams *et al.* (STAR Collaboration), Nucl. Phys. A **757**, 102 (2005).
- [3] B. I. Abelev *et al.* (STAR Collaboration), Phys. Rev. Lett. **97**, 132301 (2006).
- [4] J. Adams *et al.* (STAR Collaboration), Phys. Rev. C **71**, 064902 (2005); G. Torrieri and J. Rafelski, Phys. Lett. B **509**, 239 (2001).
- [5] J. Beringer *et al.*, (Particle Data Group) Phys. Rev. D **86**, 010001 (2012).
- [6] R. Rapp and E. V. Shuryak, Phys. Rev. Lett. B **86**, 2980 (2001).
- [7] M. Bleicher and J. Aichelin, Phys. Lett. B **530**, 81 (2002).
- [8] B.I. Abelev *et al.* (STAR Collaboration), Phys. Rev. Lett. **99**, 112301 (2007); J. Adams *et al.* (STAR Collaboration), Phys. Rev. Lett. **92**, 052302 (2004); B. I. Abelev *et al.* (STAR Collaboration), Phys. Rev. Lett. **97**, 152301 (2006); Phys. Lett. B **655**, 104 (2007). Phys. Rev. Lett. **99**, 112301 (2007).
- [9] M. Aggarwal *et al.* (STAR Collaboration) arXiv:1007.2613 [nucl-ex]; L. Kumar (for STAR Collaboration), Nucl.Phys. A **904-905**, 256c (2013).
- [10] M. Anderson, *et al.*, Nucl. Instrum. Methods **499**, 659 (2003);
- [11] B. I. Abelev *et al.* (STAR Collaboration), Phys. Rev. C **81**, 024911 (2010).
- [12] B. I. Abelev *et al.* (STAR Collaboration), Phys. Lett. B **673**, 183 (2009).
- [13] M. M. Aggarwal *et al.* (STAR Collaboration), Phys. Rev. C **84**, 034909 (2011).
- [14] B. I. Abelev *et al.* (STAR Collaboration), Phys. Rev. Lett. **99**, 112301 (2007).
- [15] B. I. Abelev *et al.* (STAR Collaboration), Phys. Rev. C **79**, 064903 (2009).
- [16] J. Adams *et al.* (STAR Collaboration), Phys. Rev. C **71**, 064902 (2005);
- [17] B. I. Abelev *et al.* (STAR Collaboration), Phys. Rev. C **78**, 044906 (2008).
- [18] J. Adams *et al.* (STAR Collaboration), Phys. Rev. Lett. **92**, 052302 (2004).
- [19] M. Nasim (for STAR Collaboration), J. Phys. Conf. Ser. **509**, 012070 (2014).
- [20] T. Hirano *et al.*, Phys. Rev. C **77**, 044909 (2008).
- [21] L. Adamczyk *et al.* (STAR Collaboration), Phys. Rev. Lett. **110**, 0142301 (2013).
- [22] BES white paper “https://drupal.star.bnl.gov/STAR/files/BES_WPII_ver6.9_cover.pdf”; M. Nasim, Phys. Rev. C **89**, 034909 (2014).
- [23] L. Kumar, Modern Physics Letters A Vol. **28**, No. 36, 1330033 (2013).
- [24] X. Zhang (for STAR Collaboration), Nucl. Phys. A **904-905**, 543c (2013).